processes

MDPI

Article

Hydrogen Production by Partial Oxidation Reforming of Methane over Ni Catalysts Supported on High and Low Surface Area Alumina and Zirconia

Anis Fakeeha [1,2], Ahmed A. Ibrahim [1], Hesham Aljuraywi [1], Yazeed Alqahtani [1], Ahmad Alkhodair [1], Suliman Alswaidan [1], Ahmed E. Abasaeed [1], Samsudeen O. Kasim [1], Sofiu Mahmud [1] and Ahmed S. Al-Fatesh [1,*]

[1] Chemical Engineering Department, College of Engineering, King Saud University, P.O. Box 800, Riyadh 11421, Saudi Arabia; anish@ksu.edu.sa (A.F.); aidid@ksu.edu.sa (A.A.I.); 435101491@student.ksu.edu.sa (H.A.); yazid_qh@hotmail.com (Y.A.); ahmeadsk@hotmail.com (A.A.); suliman.alswaidan@gmail.com (S.A.); abasaeed@ksu.edu.sa (A.E.A.); sofkolajide2@gmail.com (S.O.K.); mahmudsofiu@gmail.com (S.M.)

[2] King Abdullah City for Atomic and Renewable Energy, (K.A. CARE) Energy Research and Innovation Center at Riyadh, Riyadh 11421, Saudi Arabia

* Correspondence: aalfatesh@ksu.edu.sa; Tel.: +966-11-46-76859

Received: 7 March 2020; Accepted: 9 April 2020; Published: 25 April 2020

Abstract: The catalytic activity of the partial oxidation reforming reaction for hydrogen production over 10% Ni supported on high and low surface area alumina and zirconia was investigated. The reforming reactions, under atmospheric pressure, were performed with a feed molar ratio of CH_4/O_2 = 2.0. The reaction temperature was set to 450–650 °C. The catalytic activity, stability, and carbon formation were determined via TGA, TPO, Raman, and H_2 yield. The catalysts were calcined at 600 and 800 °C. The catalysts were prepared via the wet-impregnation method. Various characterizations were conducted using BET, XRD, TPR, TGA, TPD, TPO, and Raman. The highest methane conversion (90%) and hydrogen yield (72%) were obtained at a 650 °C reaction temperature using Ni-Al-H-600, which also showed the highest stability for the ranges of the reaction temperatures investigated. Indeed, the time-on-stream for 7 h of the Ni-Al-H-600 catalyst displayed high activity and a stable profile when the reaction temperature was set to 650 °C.

Keywords: Al_2O_3; calcination; partial oxidation; reforming of methane; supported nickel; ZrO_2

1. Introduction

Today's global energy is chiefly concentrated on power production via fossil fuels. To reduce greenhouse gas emissions, major efforts have been carried out to increase the use of renewable energy. However, the difference between renewable energy supply and energy demands necessitates further utilization of fossil fuels to supply excess energy. Fossil petroleum, commonly called natural gas, is currently employed to provide the major portion of energy requirements.

The conversion of natural gas into valuable chemical products has been the goal of several studies for some decades [1–5]. The most common processes employed to achieve such products include the transformation of methane into syngas [6,7]. Methane, an ozone depleting gas, is the main component present in natural gas. Clean energy application technologies have received much consideration in recent years because of their low emissions and high efficiencies [8–10]. The use of hydrogen as fuel for fuel cells has become the target of many investigators, as hydrogen is highly efficient, nonpolluting, and sustainable [11,12]. Owing to the great demand for H_2 and CO, for the petrochemical industry

(through the Fischer–Tropsch process to generate methanol and ammonia), hydrocarbon production, and petroleum refining processes (hydrotreating and hydrocracking), their production by the reforming of natural gas has increased significantly.

Although the main way to obtain syngas from methane on an industrial scale is from steam reforming, as presented in Equation (1), feasible alternative methods, e.g., CO_2 reforming shown in Equation (2) and the partial oxidation of methane (POM) as in Equation (3), have been investigated [13–15].

$$CH_4 + H_2O = 3H_2 + CO\ \Delta H_{298K} = 206\ \frac{kJ}{mol} \quad (1)$$

$$CH_4 + CO_2 = 2H_2 + 2CO\ \ \Delta H_{298K} = 216\ \frac{kJ}{mol} \quad (2)$$

$$CH_4 + \frac{1}{2}O_2 = 2H_2 + CO\ \Delta H_{298K} = -36\ \frac{kJ}{mol} \quad (3)$$

Both CO_2 reforming and steam reforming processes are highly endothermic and need huge energy inputs. On the other hand, the POM route has the advantage of being an exothermic process, which has a lower energy cost. POM also provides a ratio of H_2/CO = 2, which permits a straightforward syngas application for methanol or Fischer–Tropsch processes [4,14,16]. Though costly metals, like Rh, Ru, and Pt, have been employed successfully for the reactions (1–3) in terms of activity and selectivity [17–19], the high price and limited availability of the noble metals confine their applications. Instead, nickel and other transition metal-based catalysts have been stated to be active for these reactions (1–3). Nickel is preferred due to its availability, low cost, and high initial catalytic activity. Thereafter, extensive research has been performed on nickel supported over various oxides, for instance Al_2O_3 [20,21].

The prevalence of deactivation and sintering of active metals necessitates the development of Ni-based catalysts with improved activity and stability.

The partial oxidation method has the benefit of giving high conversion of methane with superb selectivity for hydrogen using relatively high space velocities [22]. Although rapid reaction kinetics and satisfactory thermodynamics are available in the literature, partial oxidation has not been commercialized yet due to challenges that include small reduction in CO selectivity caused by over oxidation that results in a local temperature rise at the catalyst surface leading to catalyst deactivation owing to its sintering and carbon formation [23]. A literature survey indicates that substantial research efforts have been dedicated to developing appropriate catalysts via numerous supports and different catalyst pretreatment methods that will increase the H_2 and CO yields. The choice of a support plays an important role in the ultimate stability of the catalysts. Dissanayake et al. investigated the partial oxidation of CH_4 using 25% Ni supported on alumina [24]. The result showed that complete conversion could be obtained if the reaction temperature was above 700 °C. The results also revealed that the catalyst bed may be subdivided into three zones with different catalytic activity aspects. Zhang et al. studied the partial oxidation of CH_4 using textural promoted alumina supported on Ni (Ni/CeO_2-ZrO_2/γ-Al_2O_3) [25]. The results indicated the effects of different preparation processes. On the other hand, Sajjadi and Haghighi examined Ni/Al_2O_3 by means of different preparation techniques, namely sol-gel, impregnation, and hybrid sol-gel plasma [26]. They found that each preparation technique possessed advantageous properties over the others, such as good dispersion, stability, coke resistance, etc.

Usually, Al_2O_3 is utilized as a support for Ni-based catalysts during reforming reactions. However, several problems are related with Al_2O_3 support; for instance, carbon deposition readily increases the catalyst deactivation, damaging of the active phase, and formation of inactive spinel phases, such as nickel aluminate ($NiAl_2O_4$) [27]. ZrO_2 is used to improve CO_2 adsorption and carbon gasification [8]. Dong et al. performed the relative investigation of partial oxidation of CH_4 over Ni/ZrO_2, Ni/CeO_2, and Ni/Ce–ZrO_2 catalysts [28]. They found that over Ni/ZrO_2, CH_4 and O_2 were activated on the surface of metallic Ni, and then adsorbed carbon reacted with adsorbed O_2 to generate CO, which designed the leading path for the partial oxidation of CH_4.

Ouaguenouni et al. investigated the preparation and catalytic activity of nickel-manganese oxide catalysts in the reaction of partial oxidation of methane [29]. In their results they found that the formation of different spinels depends on the calcination temperature. The spinel $NiMn_2O_4$ was observed to be active in the POM reaction. The catalysts calcined at 900 °C develop $NiMn_2O_4$ and give a higher CH_4 conversion, resulting from good Ni dispersion. Alternatively, Moral et al. studied the POM using Co as the active metal supported on a mixture of MgO and Al_2O_3 [30]. The authors performed the reaction at 800 °C and studied the effects of Co and MgO loadings and the calcination temperatures. Their catalysts gave CH_4 conversions of 91% using a calcination temperature of 500 °C and 20 wt.% Co and 63% MgO loadings. Kaddeche et al. examined the partial oxidation of methane on co-precipitated Ni-Mg/Al catalysts modified with copper or iron [4]. They investigated the effect of catalyst composition and pretreatment conditions of these catalysts at a 750 °C reaction temperature. The catalysts displayed very high activity and selectivity that are dependent on the conditions of preparation of the catalysts. Their results showed increased activity and selectivity with decreasing calcination temperature and increasing Ni and Al contents in the catalysts' composition. A study on Ca-decorated Al_2O_3-supported Ni and NiB catalysts, showed that the calcination temperature could significantly affect the catalyst activity [31]. A higher reduction temperature was required to ensure the complete reduction of NiO on the catalysts calcined at higher temperatures; CH_4 conversion and syngas selectivity decreased when catalysts were calcined at 800 °C.

Thus, in light of the above, it is vital to evaluate the performance of Ni catalysts with regard to supports such as alumina and zirconia by using different calcination temperatures and various operating conditions including reaction temperature and time-on-stream. Attention has been focused on the influence of catalyst performance on reactants (CH_4 and O_2) conversion and H_2 yield products in the partial oxidation reforming process. Characterizations of the spent and fresh catalysts were also performed to understand the catalytic behavior, i.e., activity and stability.

2. Experiment

2.1. Catalyst Preparation

The preparation of the desired catalysts was performed using the wet impregnation method. In the preparation of 10% nickel supported on Al_2O_3 and zirconia catalyst, 0.9 g of the support (α-Al_2O_3, γ-Al_2O_3, α-ZrO_2, or γ-ZrO_2) were impregnated with a solution having 0.495 g of ($Ni(NO_3)_2.6H_2O$) in 0.03 L of deionized H_2O. The catalyst was subjected to drying at 120 °C and calcination either at 600 or 800 °C for two hours. The catalyst was activated inside the reactor at 800 °C by passing hydrogen at a rate of 40 mL/min for 2 h followed by 20 min of N_2 at a rate of 30 mL/min. The synthesized catalysts and their corresponding designations are given in Table 1.

Table 1. Properties of the used catalysts.

Catalyst/Support	Designation	Calcination Temperature (°C)	Surface Area (m^2/g)	Pore Volume (cm^3/g)	Pore Diameter (nm)	Total H_2 Consumption (μmol/g)
α-Al_2O_3	Al-L		2.5			
10% Ni/α-Al_2O_3	Ni-Al-L-600	600	4.3	0.02	14.4	3058.9
10% Ni/α-Al_2O_3	Ni-Al-L-800	800	2.9	0.01	14.9	2637.3
γ-Al_2O_3	Al-H		260			
10% Ni/γ-Al_2O_3	Ni-Al-H-600	600	175.9	0.61	12.1	3729.8
10% Ni/γ-Al_2O_3	Ni-Al-H-800	800	146.4	0.54	13.3	4472.9
α-ZrO_2	Zr-L		22.6			
10% Ni/α-ZrO_2	Ni-Zr-L-600	600	21.5	0.16	32.0	2349.1
10% Ni/α-ZrO_2	Ni-Zr-L-800	800	15.1	0.11	33.7	3116.7
γ-ZrO_2	Zr-H		325			
10% Ni/γ-ZrO_2	Ni-Zr-H-600	600	26.7	0.16	22.5	3442.9
10% Ni/γ-ZrO_2	Ni-Zr-H-800	800	6.6	0.05	34.9	3407.5

2.2. Catalytic Reaction

The partial oxidation reaction of methane was done at atmospheric pressure in a 0.91 cm diameter and 0.30 m long stainless steel-tube fixed-bed micro reactor (the reactor is from PID Eng. & Tech Micro activity Reference Company) using 0.1 g of the catalyst. The reaction temperature was measured by a thermocouple placed in the center of the catalyst bed. The volume ratio of the feed gases (methane/oxygen/nitrogen) was 6:3:4. The total flow rate of the feed was 32.5 mL/min (i.e., 325 mL/min/gcat). The investigation was performed at reaction temperatures of 450, 500, 550, 600, and 650 °C. The effluents were analyzed using an online gas chromatograph (GC-2014 SHIMADZU) equipped with a thermal conductivity detector. The conversions of CH_4 and H_2 yield were all determined. The methane conversion and hydrogen yield were computed as:

$$CH_4 \text{ conversion } (\%) = \frac{CH_{4,in} - CH_{4,out}}{CH_{4,in}} \times 100\% \quad (4)$$

$$H_2 \textit{ Yield } (\%) = \frac{\textit{moles of } H_2 \textit{produced}}{2 \times CH_{4,in}} \times 100\% \quad (5)$$

2.3. Catalyst Characterization

Both fresh and spent catalysts were characterized by several techniques.

2.3.1. N_2 Physisorption

N_2 adsorption/desorption isotherms were used to find the textural characteristics of the catalysts, calculated at −197 °C with a Micromeritics Tristar II 3020 porosity and surface area analyzer. In each test, 200–300 mg of catalyst was taken. The samples were degassed at 300 °C for 3 h to remove undesired adsorbed gases, organics, and water vapor. The BET technique was employed to determine the surface areas.

2.3.2. XRD

X-ray diffraction (XRD) measurements for fresh catalysts were carried out. The XRD was performed using Rigaku (Miniflex), with Kα-Cu radiation at 40 kV and 40 mA. A 2θ range of 10–85° and a scanning step of 0.02° were used.

2.3.3. TPR

The activation behavior of the catalysts was investigated via an AutoChem-II Micromeritics device. For each analysis, 0.07 g of the sample were pre-treated with Ar (30 mL/ min). The samples were cooled to ambient temperature before starting the analyses. Then, the sample temperature was raised from 25 to 1000 °C in an automatic furnace at 1 atm. During temperature ramping, a H_2/Ar mixture with a volume ratio 10:90 and a flow rate of 40 mL/min was applied, while the heating rate was kept constant at 10 K/min. The outlet gases were monitored by a thermal conductivity detector (TCD) to analyze the H_2 consumption with respect to temperature.

2.3.4. TGA

The extent of the total deposited C on the used catalysts was determined using Shimadzu thermo-gravimetric analysis (TGA) in air. From the used catalysts, 0.10–0.15 g were heated at the rate of 20 °C/min from 25 to 1000 °C while recording the mass loss.

2.3.5. CO_2-TPD

The Micromeritics Autochem II apparatus was used to perform the CO_2 temperature-programmed desorption (TPD). First, 5 mg of catalyst were reduced at 600 °C for 60 min under an He flow (30 mL/min)

and then cooled to 50 °C. The CO_2 flow was continued for 1 h, and the sample was then flushed with He to remove any physisorbed CO_2. The peaks of desorption were recorded while temperature was changed by 10 °C/min. The CO_2 concentration in the effluent stream was computed using a thermal conductivity detector, and the areas under the peaks provided the amount of desorbed CO_2 during TPD.

2.3.6. TPO

Temperature program oxidation was performed in an oxidative atmosphere to determine the type of carbon deposited on the surface of the catalyst via Micromeritics AutoChem II. The analysis was executed up to 800 °C under 40 mL/min of 10% O_2/He. The used catalyst was pre-treated in the presence of Ar at 150 °C for 30 min and afterward cooled to room temperature.

2.3.7. Raman Spectroscopy

Raman spectra were carried out via an NMR-4500 Laser Raman Spectrometer. A wave length with excitation beam of 532 nm was used. An objective lens with 20× magnification was used to measure the spectra. A six mW beam power and an exposure time of 0.05 h were used. The Raman shift of the spectra was computed in the range 1000–3000 cm^{-1}. The profiles were handled by Spectra Manager Ver.2 software.

3. Results and Discussion

As a control experiment, we tested an empty reactor without catalysts under the same feed ratio and various temperatures (500–650 °C). The CH_4 conversions registered during the test were 0.0% in the 500–650 °C range. Therefore, the control experiment denoted negligible interaction of the reactor tube to the catalytic activity.

Figure 1 exhibits the catalyst N_2 adsorption/desorption isotherms, calcined at 600 °C. The catalyst N_2 isotherms fall under the type-IV classification. The isotherm is characterized by materials that are mesoporous (2–50 nm), in accordance with the International Union of Pure and Applied Chemistry (IUPAC) classification. The Ni-Al-H-600 sample has an H_2-type hysteresis loop, indicating an ink bottle type pore (mouth is narrower and back broader) whereas the Ni-Al-L-600 sample has an H3-type hysteresis, confirming non-limited adsorption. Ni-Zr-H-600 and Ni-Zr-L-600 samples have H1 hysteresis loops indicating narrower pore size distribution. It is an indication of changes in the pore patterns with different supports. Interestingly, when the calcination temperature in Figure 2 increases up to 800 °C, the pore pattern of Ni-Al-H-800 changes from H_2 to H1, indicating a change of pore pattern from ink bottle to cylindrical. The same pore pattern change from H3 to H1 is seen in of Ni-Al-L-800. Ni-Zr-H-800 and Ni-Zr-L-800 samples have the same patterns as those of the low temperature (600 °C) calcined samples. The distinctive physical structure of surface area, pore volume, and pore size are shown in Table 1. The addition of 10% nickel decreases the surface area and displays a relatively substantial effect on the specific surface area of the Ni-Zr-H-600 and Ni-Zr-H-800 catalysts. Increasing calcination temperature from 600 to 800 °C decreases the surface area and pore volume and increases the pore diameter; thus resulting in a sequence of catalysts bearing diverse inventories of hydroxyl groups. The average pore diameter of all catalysts is around 12–35 nm, which is in accord with the mesoporous characteristics of the samples.

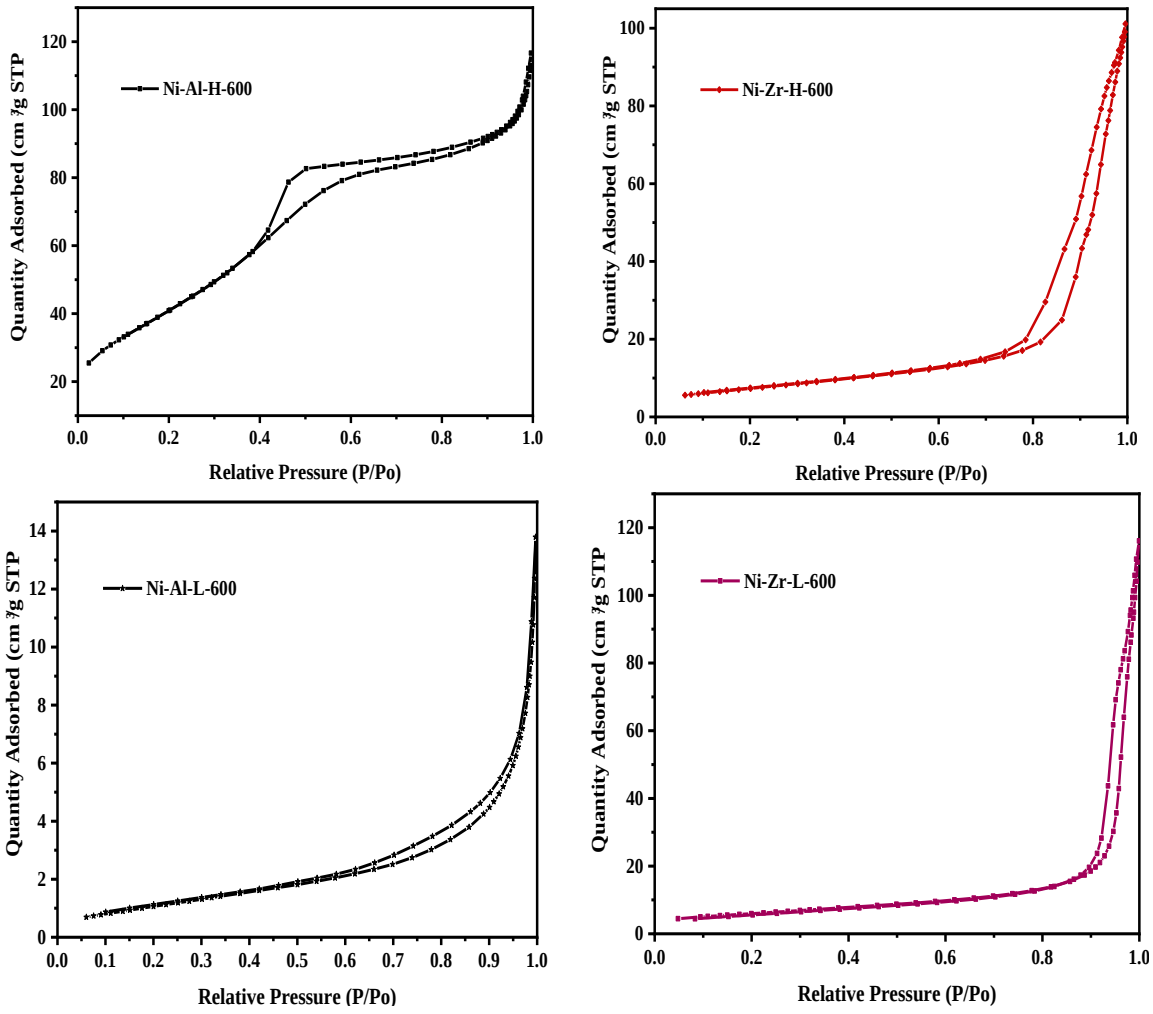

Figure 1. Nitrogen adsorption/desorption isotherms of fresh catalysts calcined at 600 °C.

Figure 3 shows the XRD spectra of catalysts pre-reduced at 600 °C for 1 h, then calcined at 600 and 800 °C. In the present study, the mesoporous alumina and zirconia were prepared by an impregnation method. Figure 3A represents the XRD pattern of Ni-Zr-L-600 and Ni-Zr-L-800. This figure shows the diffraction peaks at 2θ values of 24.7, 29.5, 32.5, 34.0, 41.0, and 50.5, which can be ascribed to the planes of (022), (111), (040), (041), (113), and (114) of L-ZrO_2 (ICSD 01-081-0610). The two catalysts have similar spectra, but the higher calcined catalyst presents somewhat higher intensities, which means crystallinity is improved. The XRD patterns of Ni-Zr-H-600 and Ni-Zr-H-800 (Figure 3B) exhibit diffraction peaks at 2θ values of 29.5, 34.7, 50.5, 60.0, 75.1, and 85.0, which were assigned to the planes of (111), (023),(114), (115), (065), and (191) of H-ZrO_2 (PDF Index 00-035-1398). In this case, the profiles are slightly different. The Ni-Zr-H-800 catalyst gives two more peaks at 2θ = 24.5 and 27.5, assigned to orthorhombic zirconia (ICSD 071964). These peaks promoted the further reduction of the surface area in comparison to less calcined samples.

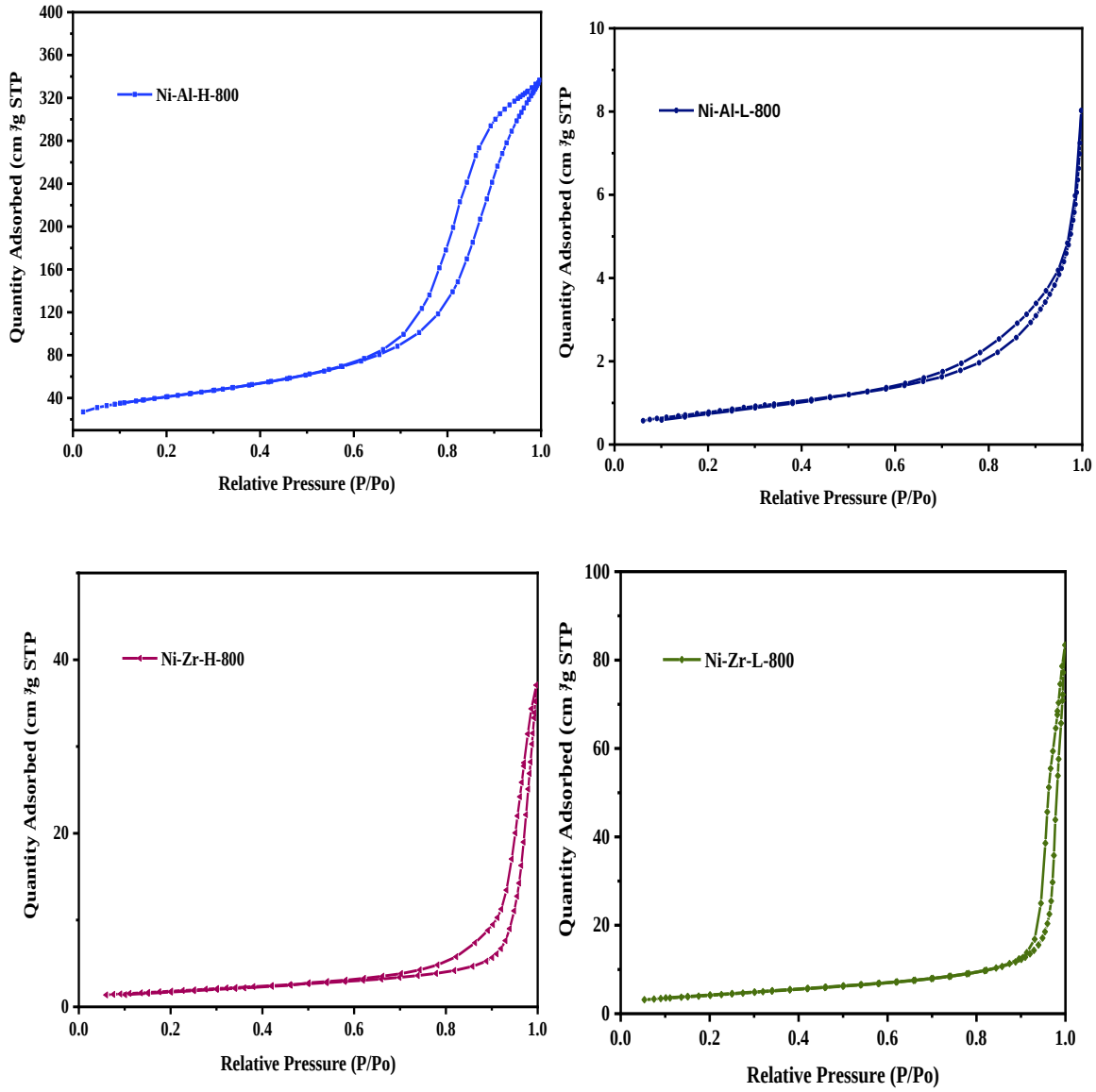

Figure 2. Nitrogen adsorption/desorption isotherms of fresh catalysts calcined at 800 °C.

The XRD patterns of Ni-Al-L-600 and Ni-Al-L-800 (Figure 3C) display diffraction peaks at 2θ values of 12.1, 26.2, 35.0, 37.2, 41.0, 53.1, 57.5, 63.3, and 68.0, which were ascribed to the planes of (101), (103), (022), (122), (303), (007), (330), (027), and (141) of L-Al_2O_3 (PDF Index 00-020-077). The effect of calcination in these samples is negligible and the profiles are almost identical. The XRD patterns of Ni-Al-H-800 and Ni-Al-H-600 (Figure 3D) display diffraction peaks at 2θ values of 19.7, 32.5, 37.2, 45.0, 60.5, 65.5, 68.0, and 85.0, which were ascribed to the planes of (111), (220), (311), (400), (511), (531), and (444) of H-Al_2O_3 (PDF Index 00-010-0339). In these catalysts, the patterns are the same, but the Ni-Al-H-800 has higher intensity, which induced further reduction of the surface area and higher pore diameter due to the higher calcination temperature. It can be inferred from the XRD results that with increasing calcination temperature, the high surface area zirconia sample achieves a high degree of crystallinity whereas the low surface area zirconia sample achieves a high intensity of the major plane. In terms of the high surface area alumina support, all peaks achieve higher intensities at higher calcination temperatures.

Figure 4 illustrates the TPR of all catalysts. The TPR results of Ni-Zr-L-600, Ni-Zr-L-800, Ni-Al-H-800, and Ni-Al-L-800 catalysts show that the peaks lie in wide ranges of temperature, which represent the characteristic reduction of stoichiometric nickel oxide [31]. Figure 4A the Zr

supported catalysts present two peaks. For instance, Ni-Zr-H-800 has peaks (maxima) at 295 °C and 460 °C, Ni-Zr-L-800 has peaks (maxima) at 314 °C and 462 °C, Ni-Zr-H-600 has peaks (maxima) at 300 °C and 486 °C and Ni-Zr-L-600 has peaks (maxima) at 482 °C and 640 °C. Low temperature (<500 °C) H_2-TPR peaks are for reduction of free NiO and it is found that Ni-Zr-L-800 and Ni-Zr-H-800 catalysts calcined at high temperatures have higher amounts of free NiO compared to the low calcined temperature samples. Intermediate temperature (<700 °C) peaks indicate moderate interaction of NiO with the support. In the Zr supported catalysts, the lower calcination temperature promotes higher interaction with the support. Figure 4B of Al supported catalysts presents single peaks, which appear at moderate or high ranges of temperature, except in the Ni-Al-L-600 catalyst, which has a prominent peak (maxima) at 360 °C. Generally, the alumina supported catalysts provide higher metal support interaction. It can be said that low temperature calcined alumina supported samples have reduction peaks in the relatively lower temperature regions than do the high temperature calcined samples. Ni-Al-L-600 has reduction peaks of free NiO whereas Ni-Al-L-800 has a reduction peak of NiO tightly interacted with its support.

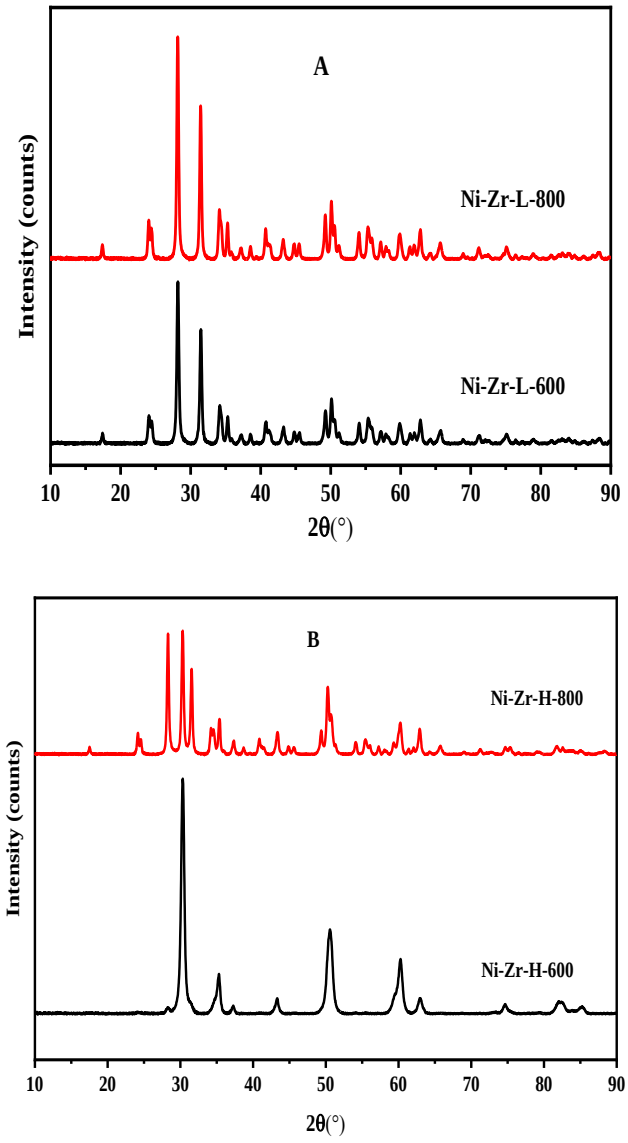

Figure 3. *Cont.*

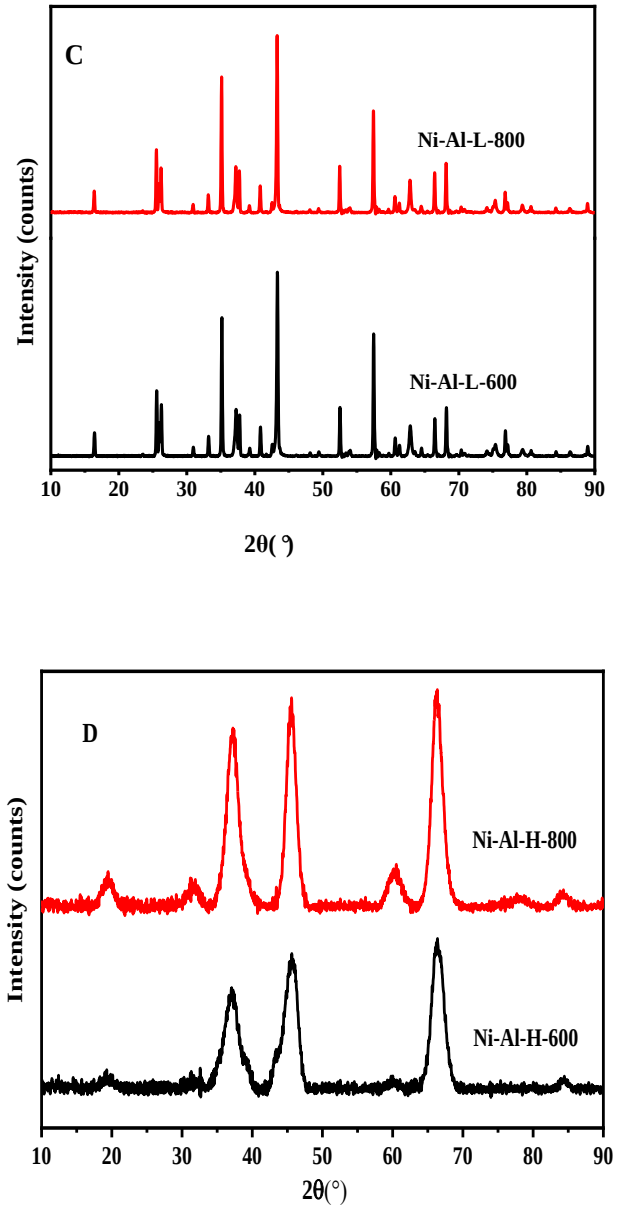

Figure 3. X-ray diffraction patterns for (**A**) Ni-Zr –L (**B**) Ni-Zr-H (**C**) Ni-Al-L (**D**) Ni-Al-H catalysts calcined at 600 and 800 °C.

In this study, CO_2-TPD was used to examine the basicity of the catalysts, as shown in Figure 5. The low surface area ZrO_2 support (Figure 5A) provides three peaks at calcination temperatures of 600 and 800 °C. Two peaks in the low temperature region, an intense peak at 100 °C and a low intensity broad peak at 260–300 °C, and a small peak in the high temperature region at 560–600 °C. On the other hand, the profile of the high surface area ZrO_2 (Figure 5A) shows three peaks for both calcination temperatures (600 and 800 °C). Two peaks in the low temperature region at 100 °C, with low and high intensity peaks for 600 and 800 °C calcination temperatures, respectively, and a distorted peak at 300–320 °C. There is a high intensity and broad peak at about 600 °C. It is fundamentally considered that the peaks at lower temperature regions can be ascribed to the weak basic sites resulting from the physical adsorption of CO_2 [32]. The peak at the high temperature associates to the strong basic sites and is accredited to the chemisorption of CO_2. As a result of the number of basic sites, the peaks have different sizes [33]. High temperature calcined samples have wide distribution of basic sites whereas the low temperature calcined samples have a concentration of the majority weak basic sites.

Figure 5B, displays the CO_2-TPD of the catalysts supported by the alumina. The profile shows four peaks for both calcinations. For the low surface area catalysts, Ni-Al-L-800 and Ni-Al-L-600, the peak sizes are very small, indicating low concentrations of basic sites. The peaks for the high surface area catalysts, Ni-Al-H-600 and Ni-Al-H-800, generated prominent, high intensity peaks, denoting significant contents of basics sites. The peaks that appeared at lower than 150 °C are ascribed to weak basic sites, while the peaks at 250–400 °C are associated with medium basic sites, and the peaks at 650–800 °C are credited to strong basic sites. It is commonly agreed that basic sites on the catalyst surface can enhance the adsorption and the dissociation of CO_2, which decreases the formation of carbon deposition to a large magnitude on active metal surface and, hence, efficiently hinders the deactivation of the catalysts. The CO_2-TPD results justify and support the supremacy of Ni-Al-H-600.

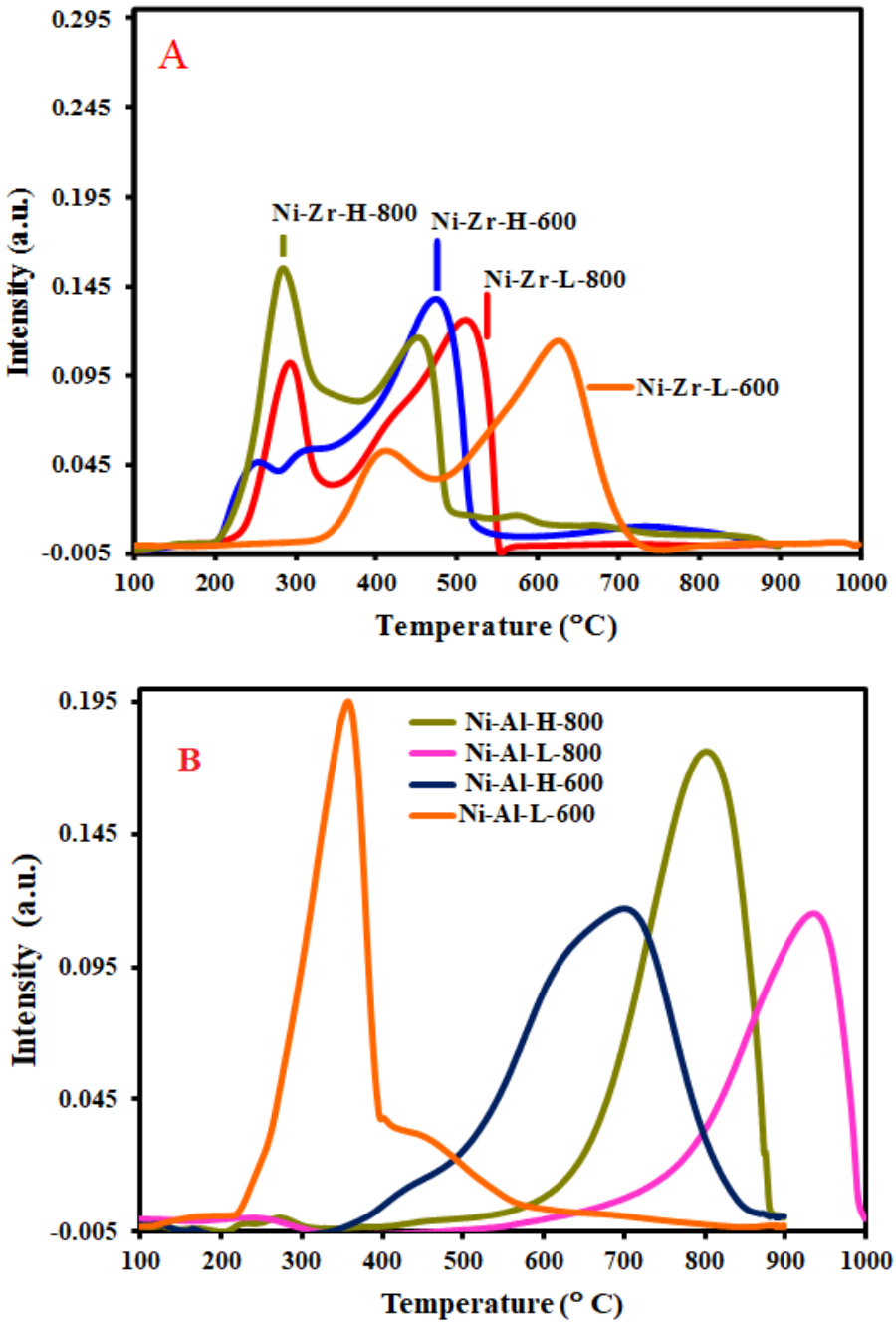

Figure 4. H_2 TPR profiles (**A**) Zr-supported catalysts, (**B**) Al-supported catalysts.

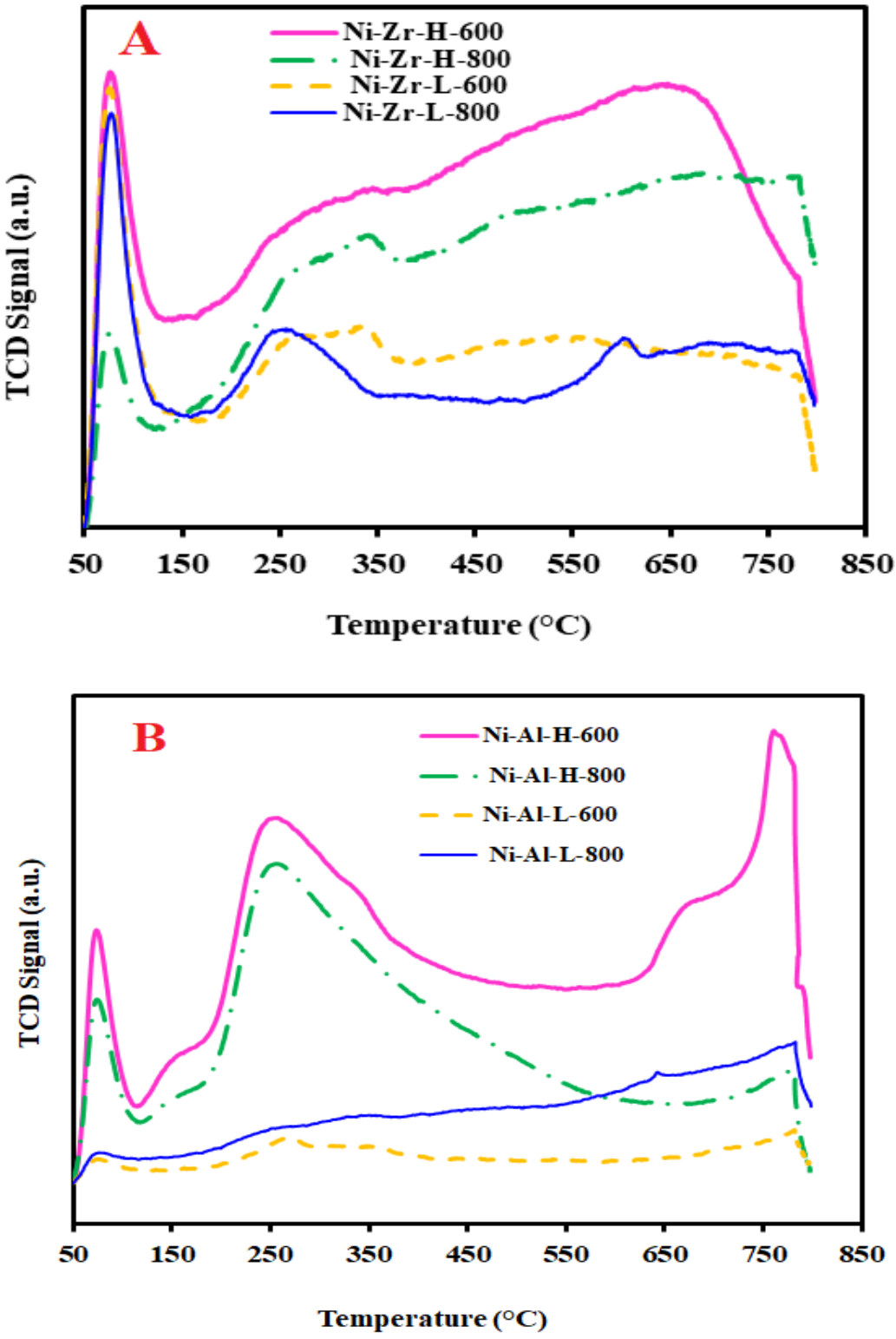

Figure 5. TPD profiles of (**A**) fresh zirconia supported- and (**B**) fresh alumina-supported catalysts calcined at 600 and 800 °C.

Figures 6–9 show the catalytic activity of 10% Ni catalysts supported on high and low surface area alumina and zirconia separately and calcined either at 600 or 800 °C. All the figures indicate CH_4 conversion and hydrogen yield profiles that increase with the increase of the reaction temperature. This is in conformity with the fact that the reaction is exothermic (heat is generated) and, therefore,

according to Le Chatelier's principle, increasing the temperature increases the products [34]. Figure 6 shows the CH_4 conversions for catalysts calcined at 600 °C. The Ni-Al-H-600 catalyst illustrates better methane conversion than the other catalysts; the conversion reached 90% at 650 °C. The performance Ni-Al-L-600 is lower than that of the corresponding Ni-Al-H-600 by 10%–34%, depending on the reaction temperature. On the other hand, the Ni-Zr-L-600 provides better conversion than that of Ni-Zr-H-600 or Ni-Al-L-600 for all reaction temperatures. Figure 7 exhibits CH_4 conversions for catalysts calcined at 800 °C. In this case the Ni-Al-H-800 catalyst offers better conversion than the other catalysts with 87% CH_4 conversion. The performance of Ni-Al-L-800 is less than the corresponding Ni-Al-H-800 by 5%–19%, depending on the reaction temperature. Alternatively, Ni-Zr-L-800 provides a slightly higher conversion than that of Ni-Zr-H-600 for most of the reaction temperatures. From Figures 6 and 7 it can be deduced that the calcination at 600 °C gives a better conversion than that at 800 °C. The high surface alumina support performs better than the low surface alumina whereas the opposite is true for the zirconia supports. Figure 8 shows the % hydrogen yield of catalysts calcined at 600 °C. Ni-Al-H-600 has the highest yield of 72%, while Ni-Zr-L-600 generates the lowest yield of 46% at 650 °C. The hydrogen yield for the Ni-Zr-H-600 catalyst is greater than that of Ni-Al-L-600. The yield profile of different catalysts is not in-line with that of the conversion. This is attributed to the drop in the selectivity of the catalysts calcined at 600 °C. Figure 9 displays the % hydrogen yield when the calcination was done at 800 °C. It indicates that Ni-Al-H-800 assumes the highest yield of 66%, while Ni-Zr-L-800 produces the lowest yield of 55% at 650 °C. The yield for the Ni-Al-L-800 catalyst is lower than that of Ni-Zr-H-800 except when the reaction temperature exceeds 620 °C. It can be concluded, from the perspective of hydrogen yield, that the higher surface area alumina calcined at 800 °C (Ni-Al-H-800) is preferable for the current process in the reaction temperature range of this study. Table 2 shows the comparison of catalytic performance of the present work and those in the literature; the table indicates the suitability of the adopted technique in this work.

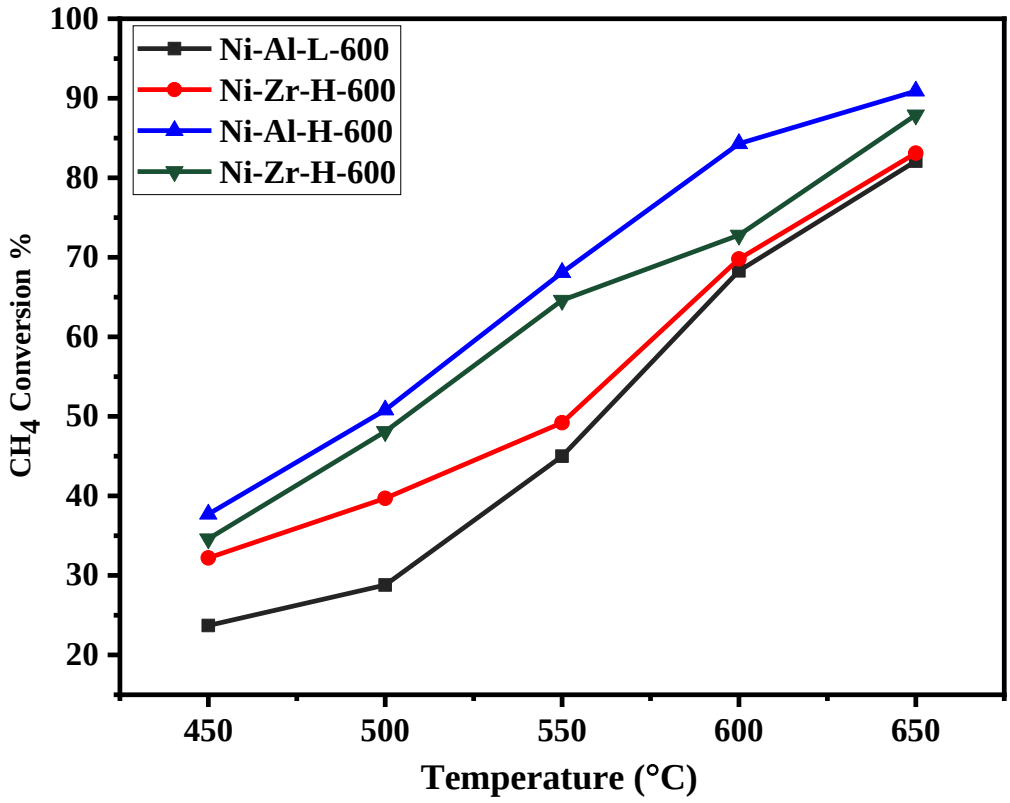

Figure 6. Catalytic activity of catalysts calcined at 600 °C: CH_4 conversion against reaction temperature (450–650 °C).

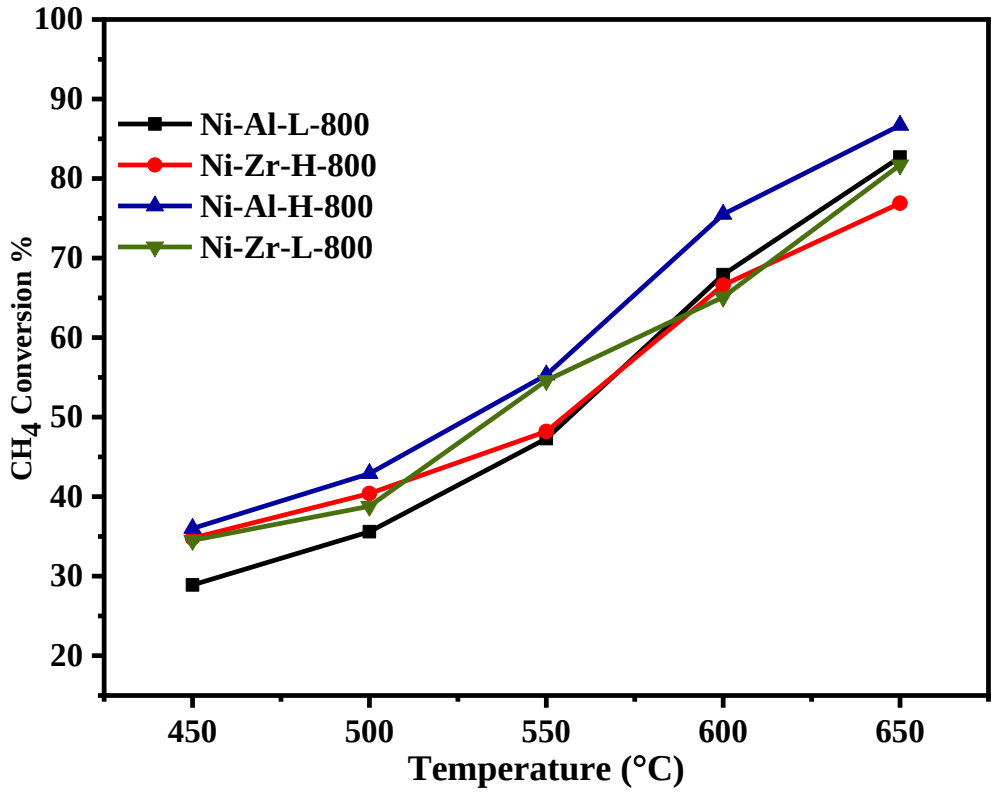

Figure 7. Catalytic activity of catalysts calcined at 800 °C: CH_4 conversion against reaction temperature (450–650 °C).

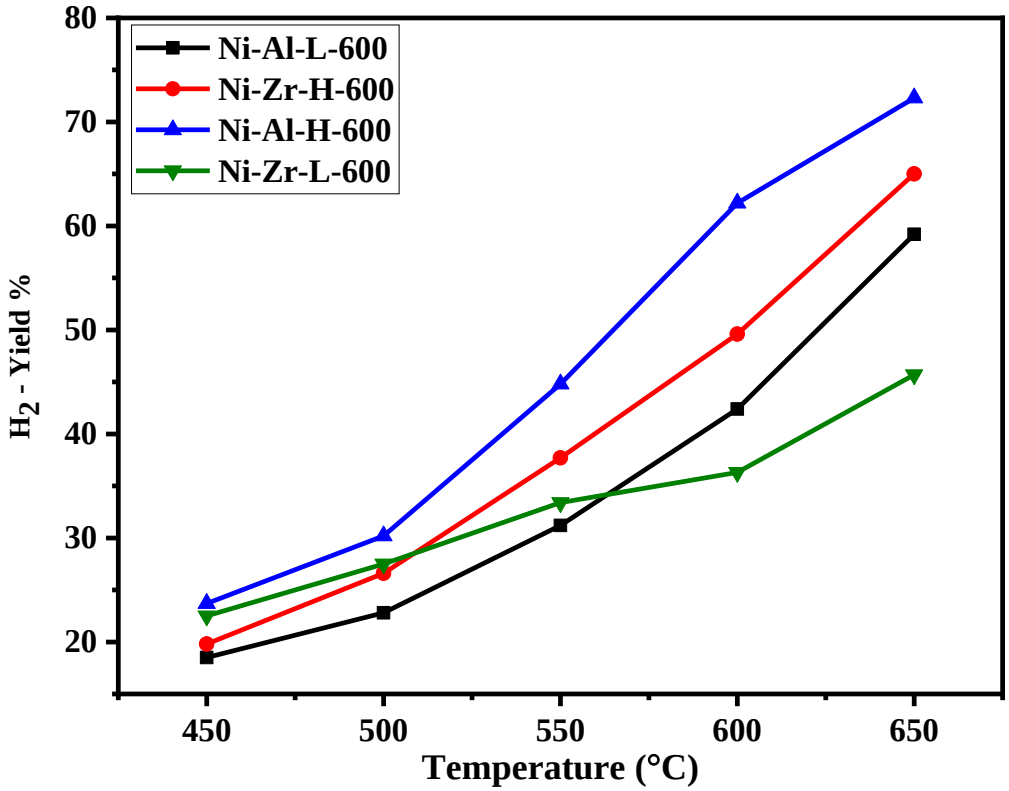

Figure 8. Catalytic activity of catalysts calcined at 600 °C: H_2 yield against reaction temperature (450–650 °C).

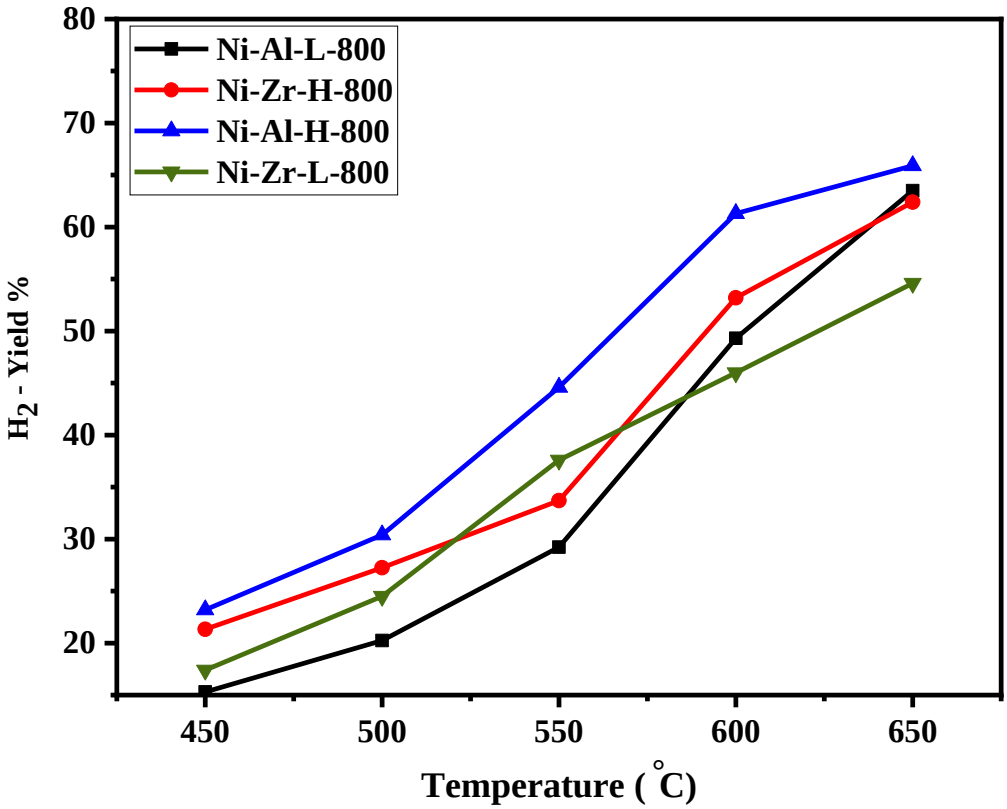

Figure 9. Catalytic activity of catalysts calcined at 800 °C: H_2 yield against reaction temperature (450–650 °C).

Table 2. Comparison of catalytic performance of partial oxidation of methane.

Catalyst	Weight (g)	CH_4:O_2	Space Velocity (mL/g/h)	Reaction Temperature (°C)	% CH_4 Conversion	Reference
25% Ni/Al_2O_3+TiO_2+CaO	0.05	1.78:1.00	6×10^4	650	86	[24]
10% $Ni/Ce_{0.7}Zr_{0.3}O_2$-Al_2O_3	0.5	2.00:1.00	4×10^4	650	67.8	[25]
La_2NiZrO_6	0.01	2.00:1.00	300×10^4	750	40	[35]
8% Ni/CeO_2-ZrO_2-Al_2O_3	0.15	2.00:1.00	20×10^4	650	88.5	[36]
6% Ni/SiO_2	0.1	2.00:1.00	6×10^4	600	85	[37]
Ni-Al-H-600	0.1	2.00:1.00	1.95×10^4	650	90	This work

Figure 10A shows the weight loss of the used catalysts, calcined at 600 °C, and operated for 5 h. The profile shows the nonexistence of desorption of strongly adsorbed water and oxidation of volatile organic compounds since no weight loss below 650 °C was detected. The weight loss observed over 650 °C was alike for all catalysts and attributed to the oxidation of graphitic carbon species [38,39]. For the Ni-Al-L-600 and Ni-Al-H-600 catalysts, the weight loss was about 8.6% and 6.0%, respectively, justifying the different conversions obtained with these two catalysts. While for the Ni-Zr-L-600 and Ni-Zr-H-600 catalysts, the weight loss was about 2.3% and 5.5%, respectively. Figure 10B shows the weight loss of the used catalysts, calcined at 800 °C, and operated for 5 h. The weight losses are quite low: Ni-Al-H-800, Ni-Al-L-800, Ni-Zr-L-800, and Ni-Zr-H-800 give weight losses of approximately 7.0%, 0.9%, 5.2%, and 1.0%, respectively.

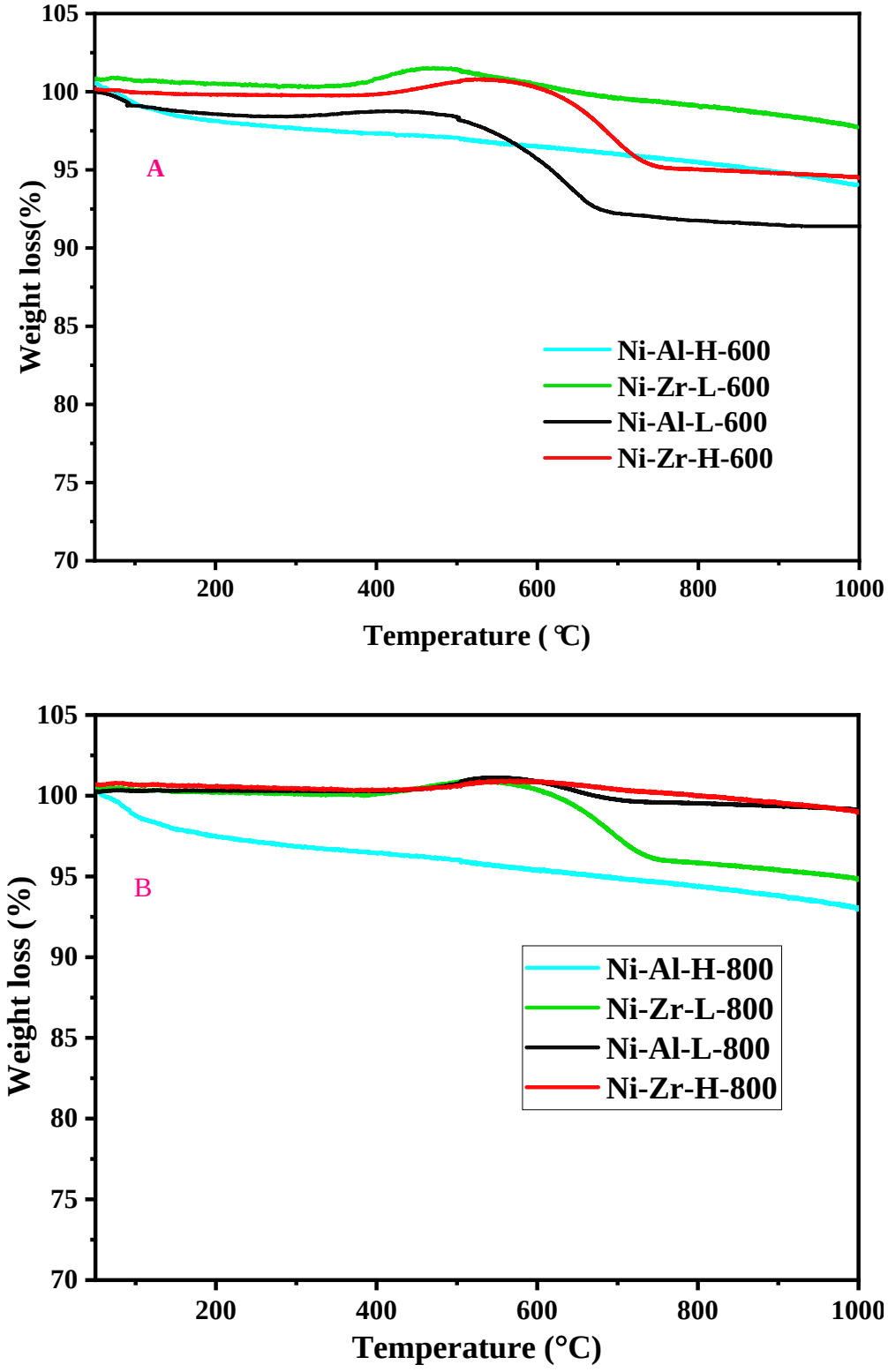

Figure 10. TGA shapes of the spent calcined at (**A**) 600 °C and (**B**) 800 °C, operated for 5 h, during the reaction at 450–650 °C.

Figure 11 exhibits the CH_4 conversion and H_2-yield profiles of the Ni-Al-H-600 catalyst for different reaction temperatures for about 7 h time-on-stream. Figure 11A shows methane conversion against time-on-stream for different reaction temperatures. The best CH_4 conversion of 90% and

the highest stability is attained using a 650 °C reaction temperature, while 52% CH_4 conversion is recorded for a 500 °C reaction temperature. The conversion enhances with the increase of the reaction temperature, since rates of reaction increase with increase of temperature. The 650 °C gives not only excellent activity but also excellent stability. Therefore, the time-on-stream analysis indicates that the 650 °C reaction temperature results in the best performance of the of Ni-Al-H-600 catalyst. Figure 11B shows hydrogen yield against time-on-stream for different reaction temperatures. The highest H_2 yield of 72% and the best stability is obtained at a 650 °C reaction temperature, while the lowest H_2 yield of 28% is registered for 500 °C.

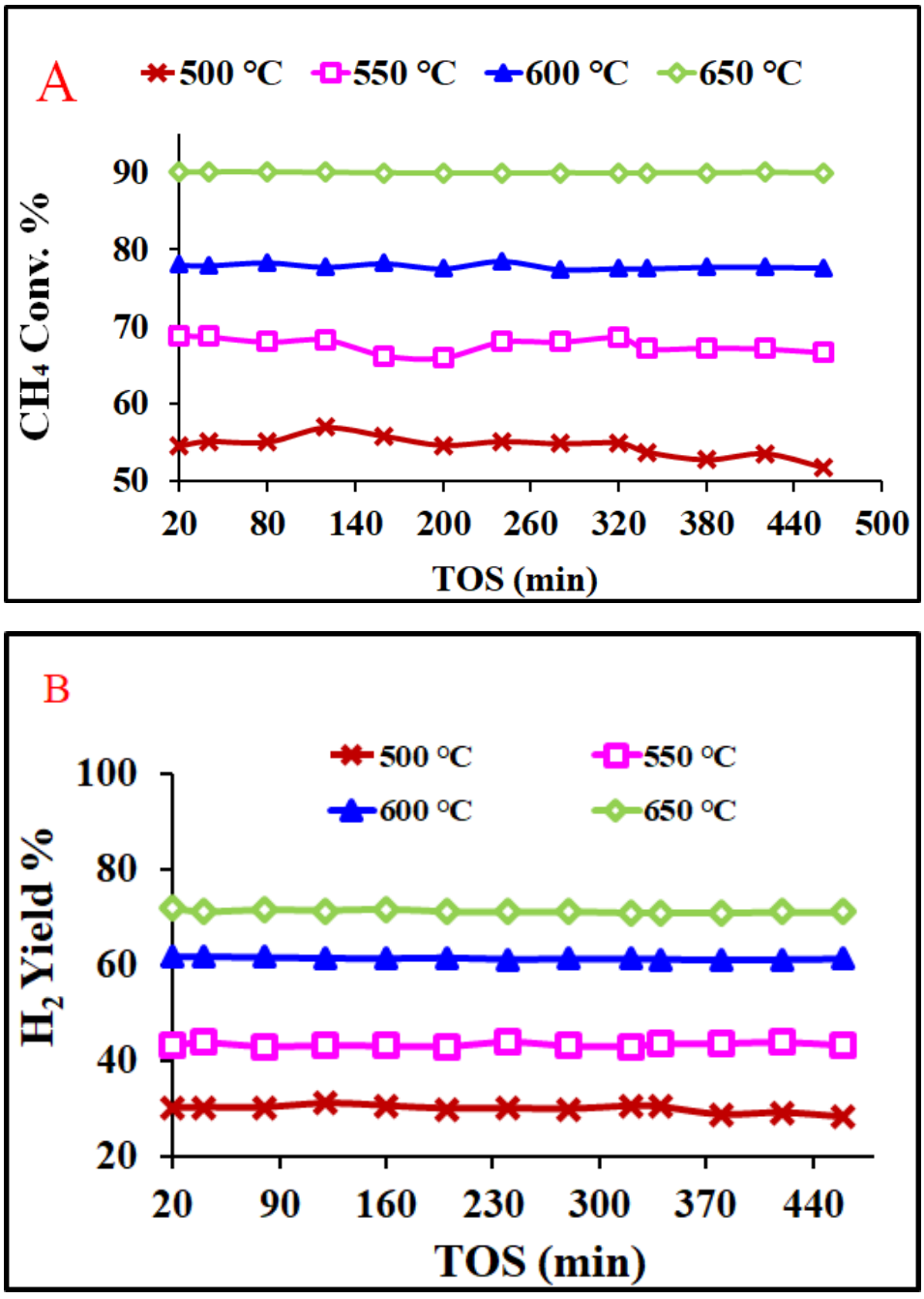

Figure 11. (**A**) Conversions of CH_4 and (**B**) H_2 yield during a 7 h stability test of the Ni-Al-H-600 catalyst; activation 750 °C; reaction temperatures (500–650 °C), F/W = 19,500 mL/g-cat.

Figure 12 shows the TPO profiles of the spent Ni-Al-H-600 catalyst operated for 5 h at different reaction temperatures. The figure shows peaks of CO_2 desorption at lower temperatures for all reaction temperatures corresponding to atomic and amorphous carbonaceous species. At the high reaction temperatures of 600 and 650 °C, there is an additional peak corresponding to graphitic carbonaceous species. The negative peaks around at around 250–300 °C are ascribed to the oxidation of the metallic nickel and its intensity is diminished with the increase of reaction temperature. Therefore for the same catalyst, increasing the reaction temperature above 550 °C induces the formation of graphitic carbon, whereas the different oxidation regions result from the different locations of the carbon on the surface of the catalyst. Carbon deposition is an essential feature of reforming reactions. The different carbon structures are customarily assessed by Raman analysis. Figure 13 depicts the Raman spectra of spent Ni-Al-H-600 catalysts acquired for 7 h using reaction temperatures of 500, 550, 600, and 650 °C. Two comparable intensity peaks appeared at 1475 cm^{-1} and 1535 cm^{-1}, corresponding to the D band, assigned to sp3 hybridized amorphous carbon, and G band, specified by the presence of graphitized carbon, respectively. The D band and G band are typical bands of regular-structured carbon that form on the surface of Ni-Al-H-600 during the partial reforming reaction. The results of Raman analysis confirm the formation of different types of carbon, particularly for high reaction temperatures, as is illustrated in the TPO analysis. Figure 14 illustrates the TGA analysis of the Ni-Al-H-600 catalyst operated at different reaction temperatures that lasted for 5 h. The result shows 4% weight loss of the mass due to gasification of the gas formed on the catalyst when the reaction temperature was 500 °C, while 8% weight loss was determined using a reaction temperature of 650 °C. As the reaction temperature was increased, the production of carbon grew slightly as a result of increased decomposition of CH_4.

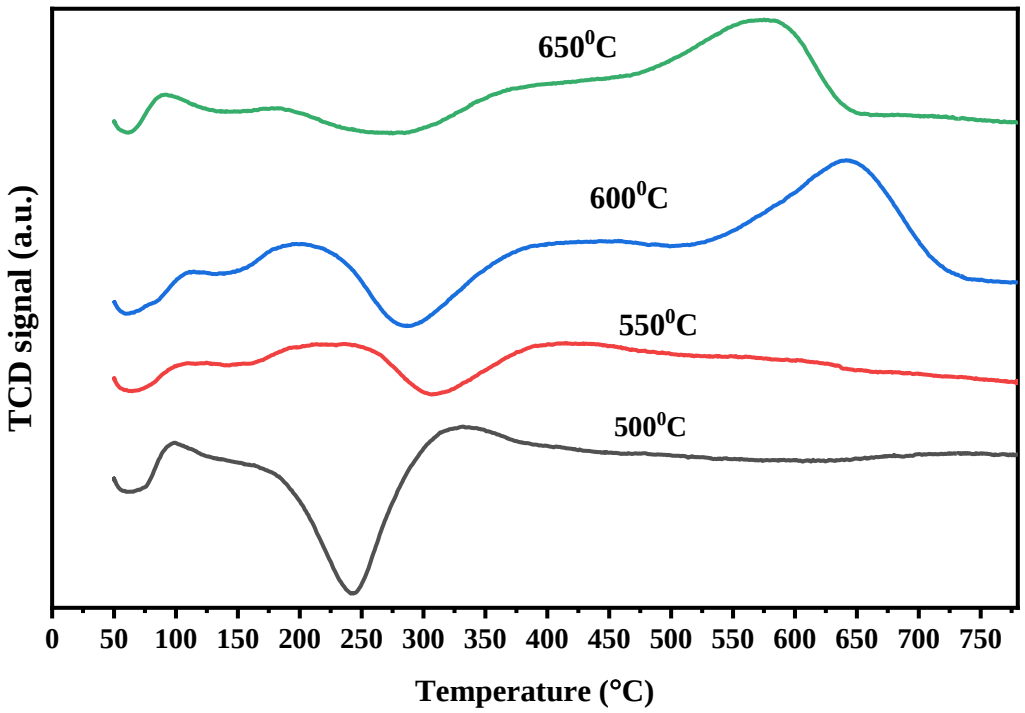

Figure 12. TPO profiles of the Ni-Al-H-600 catalyst after 7 h reaction temperature operated at different values (500, 550, 600, and 650 °C).

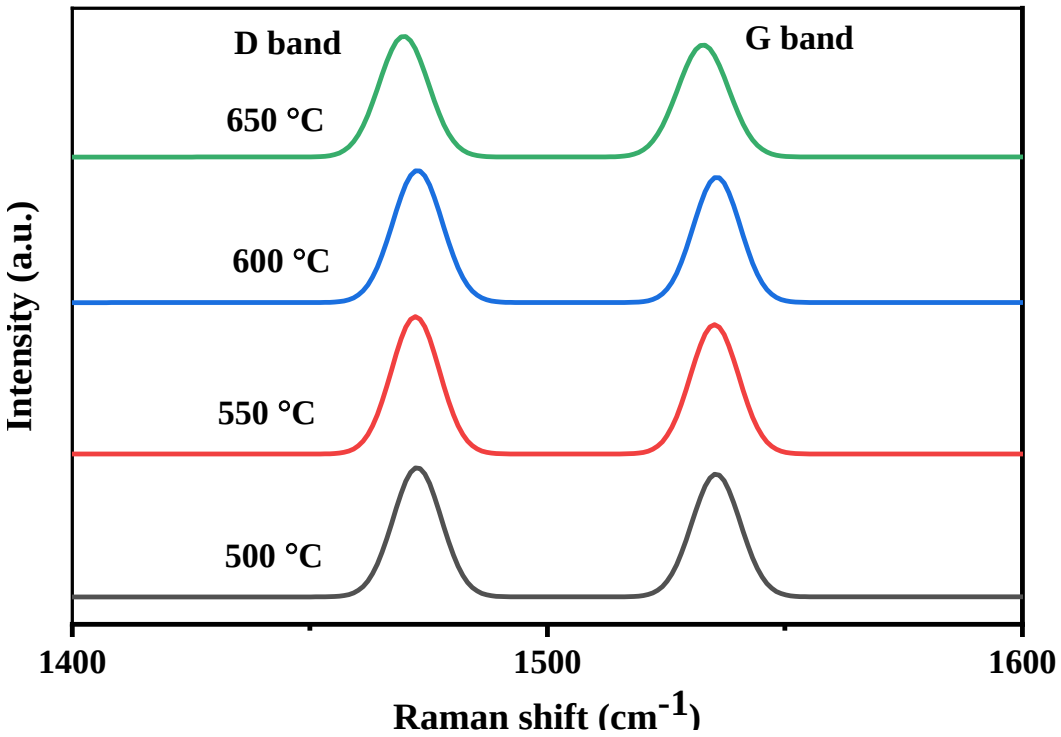

Figure 13. Raman spectra of the Ni-Al-H-600 catalyst obtained at different reaction temperatures (500, 550, 600, and 650 °C).

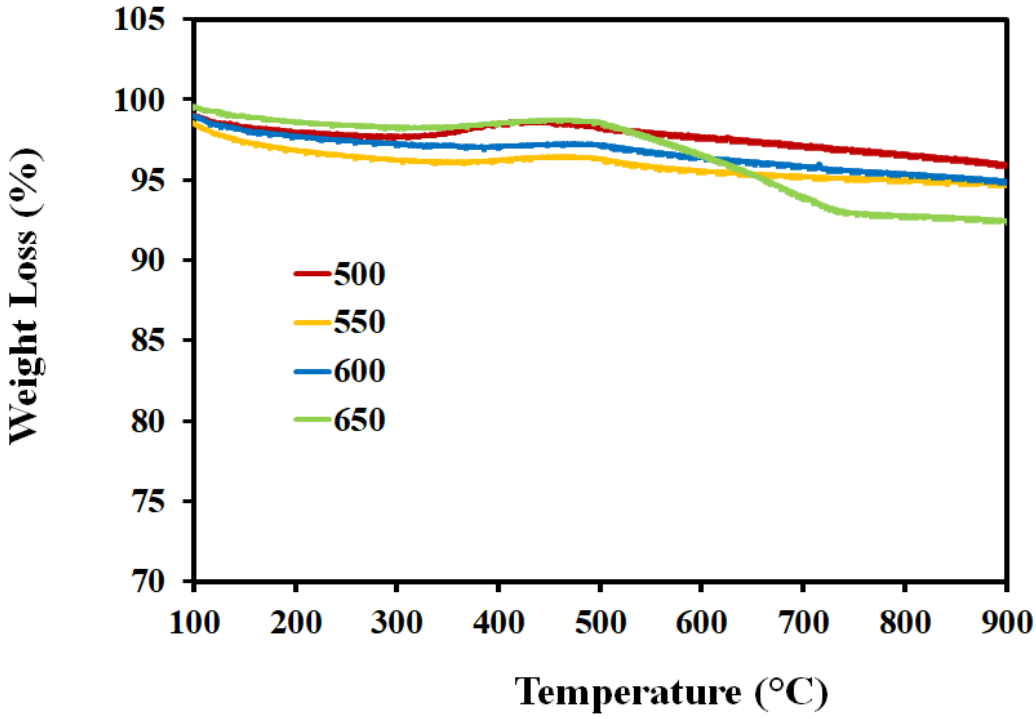

Figure 14. TGA analysis of the Ni-Al-H-600 catalyst obtained at different reaction temperatures for 7 h.

4. Conclusions

Different calcined 10% Ni catalysts supported on both high and low Al_2O_3 and on both high and low ZO_2 were tested for partial oxidation reforming of methane. The catalysts were calcined at 600 and 800 °C. The highest CH_4 conversion of 90% and H_2 yield of 72% were obtained using Ni-Al-H-600.

The Ni-Al-H-600 catalyst retained the maximum surface area and the biggest pore volume. The study of the TGA indicated low amounts of carbon deposition except for the Ni-Al-L-600 catalyst. The TPO and Raman analyses of the catalysts denoted the presence of different types of carbon. The best activity and stability of performance of the Ni-Al-H-600 catalyst over different reaction temperatures (500–650 °C) was attained when the reaction was conducted at 650 °C for the period of 7 h.

Author Contributions: Experiment and Writing—original draft preparation A.F., A.A.I., A.S.A.-F., and S.O.K.; XRD analysis S.M., Preparation of catalyst, A.S.A.-F., H.A., Y.A., A.A., and S.A., Writing—review and editing, A.E.A. and A.F. All authors have read and agreed to the published version of the manuscript.

Funding: The work is supported by the Deanship of Scientific Research programs of King Saud University via project No. RGP-119.

Acknowledgments: The KSU authors would like to extend their sincere appreciation to the Deanship of Scientific Research at the King Saud University for its funding for this research group project # RGP-119.

Conflicts of Interest: The authors declare no conflict of interest.

References

1. He, S.; Castello, D.; Krishnamurthy, K.R.; Al-Fatesh, A.S.; Winkelman, J.G.M.; Seshan, K.; Fakeeha, A.H.; Kersten, S.R.A.; Heeres, H.J. Kinetics of long chain n-paraffin dehydrogenation over a commercial Pt-Sn-K-Mg/γ-Al_2O_3 catalyst: Model studies using n-dodecane. *Appl. Catal. A Gen.* **2019**, *579*, 130–140. [CrossRef]
2. Vermeiren, W.J.M.; Blomsma, E.; Jacobs, P.A. Catalytic and thermodynamic approach of the oxyreforming reaction of methane. *Catal. Today* **1992**, *13*, 427–436. [CrossRef]
3. Gillessen, B.; Heinrichs, H.; Hake, J.F.; Allelein, H.J. Natural gas as a bridge to sustainability: Infrastructure expansion regarding energy security and system transition. *Appl. Energy* **2019**, *251*, 113377. [CrossRef]
4. Kaddeche, D.; Djaidja, A.; Barama, A. Partial oxidation of methane on co-precipitated Ni–Mg/Al catalysts modified with copper or iron. *Int. J. Hydrog. Energy* **2017**, *42*, 15002–15009. [CrossRef]
5. Pruksawan, S.; Kitiyanan, B.; Ziff, R.M. Partial oxidation of methane on a nickel catalyst: Kinetic Monte-Carlo simulation study. *Chem. Eng. Sci.* **2016**, *147*, 128–136. [CrossRef]
6. Pantaleo, G.; Parola, V.L.; Deganello, F.; Singha, R.K.; Bal, R.; Venezia, A.M. Ni/CeO_2 catalysts for methane partial oxidation: Synthesis driven structural and catalytic effects. *Appl. Catal. B Environ.* **2016**, *189*, 233–241. [CrossRef]
7. Gao, H.; Zhou, L.; Luo, X.; Liang, Z. Optimized process configuration for CO_2 recovery from crude synthesis gas via a rectisol wash process. *Int. J. Greenh. Gas Control* **2018**, *79*, 83–90. [CrossRef]
8. Zhang, L.; Zhang, Q.; Liu, Y.; Zhang, Y. Dry reforming of methane over Ni/MgO-Al_2O_3 catalysts prepared by two-step hydrothermal method. *Appl. Surf. Sci.* **2016**, *389*, 25–33. [CrossRef]
9. Al-Fatesh, A.S.; Abu-Dahrieh, J.K.; Atia, H.; Armbruster, U.; Ibrahim, A.A.; Khan, W.U.; Abasaeed, A.E.; Fakeeha, A.H. Effect of pre-treatment and calcination temperature on Al_2O_3-ZrO_2 supported Ni-Co catalysts for dry reforming of methane. *Int. J. Hydrog. Energy* **2019**, *44*, 21546–21558. [CrossRef]
10. Yang, W.; Fan, A.; Yao, H.; Liu, W. Effect of reduced pressures on the combustion efficiency of lean H_2/air flames in a micro cavity-combustor. *Int. J. Hydrog. Energy* **2016**, *41*, 15354–15361. [CrossRef]
11. Gan, Y.; Luo, Y.; Wang, M.; Shi, Y.; Yan, Y. Effect of alternating electric fields on the behaviour of small-scale laminar diffusion flames. *Appl. Therm. Eng.* **2015**, *89*, 306–315. [CrossRef]
12. Radfarnia, H.R.; Iliuta, M.C. Hydrogen production by sorption-enhanced steam methane reforming process using CaO-Zr/Ni bifunctional sorbent–catalyst. *Chem. Eng. Process. Process Intensif.* **2014**, *86*, 96–103. [CrossRef]
13. Kaczmarek, D.; Atakan, B.; Kasper, T. Investigation of the partial oxidation of methane/n-heptane-mixtures and the interaction of methane and n-heptane under ultra-rich conditions. *Combust. Flame* **2019**, *205*, 345–357. [CrossRef]
14. Melchiori, T.; Di Felice, L.; Mota, N.; Navarro, R.M.; Fierro, J.L.G.; Annaland, M.V.S.; Gallucci, F. Methane partial oxidation over a LaCr0.85Ru0.15O_3 catalyst: Characterization, activity tests and kinetic modeling. *Appl. Catal. A Gen.* **2014**, *486*, 239–249. [CrossRef]

15. Costa, D.S.; Gomes, R.S.; Rodella, C.B.; da Silva, R.B.; Fréty, R.; Teixeira Neto, É.; Brandão, S.T. Study of nickel, lanthanum and niobium-based catalysts applied in the partial oxidation of methane. *Catal. Today* **2018**. [CrossRef]
16. Wang, F.; Li, W.-Z.; Lin, J.-D.; Chen, Z.-Q.; Wang, Y. Crucial support effect on the durability of $Pt/MgAl_2O_4$ for partial oxidation of methane to syngas. *Appl. Catal. B Environ.* **2018**, *231*, 292–298. [CrossRef]
17. Hou, Z.; Chen, P.; Fang, H.; Zheng, X.; Yashima, T. Production of synthesis gas via methane reforming with CO_2 on noble metals and small amount of noble-(Rh-) promoted Ni catalysts. *Int. J. Hydrog. Energy* **2006**, *31*, 555–561. [CrossRef]
18. Fasolini, A.; Abate, S.; Barbera, D.; Centi, G.; Basile, F. Pure H_2 production by methane oxy-reforming over Rh-Mg-Al hydrotalcite-derived catalysts coupled with a Pd membrane. *Appl. Catal. A Gen.* **2019**, *581*, 91–102. [CrossRef]
19. Araújo, J.C.S.; Oton, L.F.; Bessa, B.; Neto, A.B.S.; Oliveira, A.C.; Lang, R.; Otubo, L.; Bueno, J.M.C. The role of Pt loading on La_2O_3-Al_2O_3 support for methane conversion reactions via partial oxidation and steam reforming. *Fuel* **2019**, *254*, 115681. [CrossRef]
20. Zhao, A.; Ying, W.; Zhang, H.; Ma, H.; Fang, D. Ni–Al_2O_3 catalysts prepared by solution combustion method for syngas methanation. *Catal. Commun.* **2012**, *17*, 34–38. [CrossRef]
21. Song, Y.; Liu, H.; Liu, S.; He, D. Partial Oxidation of Methane to Syngas over Ni/Al_2O_3 Catalysts Prepared by a Modified Sol−Gel Method. *Energy Fuels* **2009**, *23*, 1925–1930. [CrossRef]
22. Beretta, A.; Bruno, T.; Groppi, G.; Tavazzi, I.; Forzatti, P. Conditioning of Rh/α-Al_2O_3 catalysts for H2 production via CH4 partial oxidation at high space velocity. *Appl. Catal. B Environ.* **2007**, *70*, 515–524. [CrossRef]
23. Jing, Q.; Zheng, X.J.E. Combined catalytic partial oxidation and CO_2 reforming of methane over ZrO_2-modified Ni/SiO_2 catalysts using fluidized-bed reactor. *Energy* **2006**, *31*, 2184–2192. [CrossRef]
24. Dissanayake, D.; Rosynek, M.P.; Kharas, K.C.C.; Lunsford, J.H.L. Partial oxidation of methane to carbon monoxide and hydrogen over a Ni/Al_2O_3 catalyst. *J. Catal.* **1991**, *132*, 117–127. [CrossRef]
25. Zhang, Q.; Shen, M.; Wen, J.; Wang, J.; Fei, Y. Partial oxidation of methane on Ni/CeO_2-ZrO_2/γ- Al_2O_3 prepared using different processes. *J. Rare Earths* **2008**, *26*, 347–351. [CrossRef]
26. Sajjadi, S.M.; Haghighi, M. Impregnation vs. sol-gel and sol-gel-plasma dispersion of nickel nanoparticles over Al_2O_3 employed in combined dry reforming and partial oxidation of greenhouse gases to syngas. *Int. J. Hydrog. Energy* **2018**, *43*, 15014–15029. [CrossRef]
27. Wu, P.; Li, X.; Ji, S.; Lang, B.; Habimana, F.; Li, C. Steam reforming of methane to hydrogen over Ni-based metal monolith catalysts. *Catal. Today* **2009**, *146*, 82–86. [CrossRef]
28. Dong, W.-S.; Jun, K.-W.; Roh, H.-S.; Liu, Z.-W.; Park, S.-E. Comparative study on partial oxidation of methane over Ni/ZrO_2, Ni/CeO_2 and Ni/Ce–ZrO_2, catalysts. *Catal. Lett.* **2002**, *78*, 215–222. [CrossRef]
29. Hadj-Sadok Ouaguenouni, M.; Benadda, A.; Kiennemann, A.; Barama, A. Preparation and catalytic activity of nickel–manganese oxide catalysts in the reaction of partial oxidation of methane. *Comptes Rendus Chim.* **2009**, *12*, 740–747. [CrossRef]
30. Moral, A.; Reyero, I.; Llorca, J.; Bimbela, F.; Gandía, L.M. Partial oxidation of methane to syngas using Co/Mg and Co/Mg-Al oxide supported catalysts. *Catal. Today* **2019**, *333*, 259–267. [CrossRef]
31. Chen, L.; Lu, Y.; Hong, Q.; Lin, J.; Dautzenberg, F.M. Catalytic partial oxidation of methane to syngas over Ca-decorated-Al2O3-supported Ni and NiB catalysts. *Appl. Catal. A Gen.* **2005**, *292*, 295–304. [CrossRef]
32. Wierzbicki, D.; Baran, R.; Dębek, R.; Motak, M.; Gálvez, M.E.; Grzybek, T.; Da Costa, P.; Glatzel, P. Examination of the influence of La promotion on Ni state in hydrotalcite-derived catalysts under CO_2 methanation reaction conditions: Operando X-ray absorption and emission spectroscopy investigation. *Appl. Catal. B Environ.* **2018**, *232*, 409–419. [CrossRef]
33. Li, D.; Li, R.; Lu, M.; Lin, X.; Zhan, Y.; Jiang, L. Carbon dioxide reforming of methane over Ru catalysts supported on Mg-Al oxides: A highly dispersed and stable Ru/Mg(Al)O catalyst. *Appl. Catal. B Environ.* **2017**, *200*, 566–577. [CrossRef]
34. Chatelier, H.L.L. Sur un énoncé général des lois des équilibres chimiques. *Comptes Rendus Chim.* **1884**, *99*, 786–789.
35. Ma, Y.; Ma, Y.; Chen, Y.; Ma, S.; Li, Q.; Hu, X.; Wang, Z.; Buckley, C.E.; Dong, D. Highly stable nanofibrous La_2NiZrO_6 catalysts for fast methane partial oxidation. *Fuel* **2020**, *265*, 116861. [CrossRef]

36. Dajiang, M.; Yaoqiang, C.; Junbo, Z.; Zhenling, W.; Di, M.; Maochu, G. Catalytic Partial Oxidation of Methane over Ni/CeO_2-ZrO_2-Al_2O_3. *J. Rare Earths* **2007**, *25*, 311–315. [CrossRef]
37. Emamdoust, A.; La Parola, V.; Pantaleo, G.; Testa, M.L.; Shayesteh, S.F.; Venezia, A.M. Partial oxidation of methane over SiO_2 supported Ni and NiCe catalysts. *J. Energy Chem.* **2020**, *47*, 1–9. [CrossRef]
38. Padilla, R.; Benito, M.; Rodríguez, L.; Serrano, A.; Muñoz, G.; Daza, L. Nickel and cobalt as active phase on supported zirconia catalysts for bio-ethanol reforming: Influence of the reaction mechanism on catalysts performance. *Int. J. Hydrog. Energy* **2010**, *35*, 8921–8928. [CrossRef]
39. Ding, M.; Tu, J.; Zhang, Q.; Wang, M.; Tsubaki, N.; Wang, T.; Ma, L. Enhancement of methanation of bio-syngas over CeO2-modified Ni/Al2O3 catalysts. *Biomass Bioenergy* **2016**, *85*, 12–17. [CrossRef]

© 2020 by the authors. Licensee MDPI, Basel, Switzerland. This article is an open access article distributed under the terms and conditions of the Creative Commons Attribution (CC BY) license (http://creativecommons.org/licenses/by/4.0/).